Biomedicine & Pharmacotherapy 158 (2023) 114070

Contents lists available at ScienceDirect

Biomedicine & Pharmacotherapy

journal homepage: www.elsevier.com/locate/biopha

The synthetic molecule stauprimide impairs cell growth and migration in triple-negative breast cancer

P. Carrillo [a,b,1], M. Bernal [a,b,1], C. Téllez-Quijorna [a], A.D. Marrero [a,b], I. Vidal [a,b], L. Castilla [a,b], C. Caro [b], A. Domínguez [b], M.L. García-Martín [b,c], A.R. Quesada [a,b,d], M.A. Medina [a,b,d], B. Martínez-Poveda [a,b,e,*]

[a] Departamento de Biología Molecular y Bioquímica, Facultad de Ciencias, Universidad de Málaga, Andalucía Tech, E-29071 Málaga, Spain
[b] Instituto de Investigación Biomédica de Málaga y Plataforma en Nanomedicina (IBIMA Plataforma BIONAND), C/Severo Ochoa, 35, 29590, Málaga, Spain
[c] Biomedical Research Networking Center in Bioengineering, Biomaterials & Nanomedicine (CIBER-BBN), Spain
[d] CIBER de Enfermedades Raras (CIBERER, Instituto de Salud Carlos III), Spain
[e] CIBER de Enfermedades Cardiovasculares (CIBERCV, Instituto de Salud Carlos III, Madrid), Spain

ARTICLE INFO

Keywords:
Stauprimide
Triple-negative breast cancer
Antitumoral compound
Proliferation
Migration

ABSTRACT

Stauprimide, a semi-synthetic derivative of staurosporine, is known mainly for its potent differentiation-enhancing properties in embryonic stem cells. Here, we studied the effects of stauprimide in cell growth and migration of triple-negative breast cancer cells *in vitro*, evaluating its potential antitumoral activity in an orthotopic mouse model of breast cancer *in vivo*. Our results from survival curves, EdU incorporation, cell cycle analysis and annexin-V detection in MDA-MB-231 cells indicated that stauprimide inhibited cell proliferation, arresting cell cycle in G_2/M without induction of apoptosis. A decrease in the migratory capability of MDA-MB-231 was also assessed in response to stauprimide. In this work we pointed to a mechanism of action of stauprimide involving the modulation of ERK1/2, Akt and p38 MAPK signalling pathways, and the downregulation of *MYC* in MDA-MB-231 cells. In addition, orthotopic MDA-MB-231 xenograft and 4T1 syngeneic models suggested an effect of stauprimide *in vivo*, increasing the necrotic core of tumors and reducing metastasis in lung and liver of mice. Together, our results point to the promising role of stauprimide as a putative therapeutic agent in triple-negative breast cancer.

1. Introduction

Breast cancer is the leading cause of cancer incidence in 2020, representing 11.7 % of cancer cases worldwide, and accounting for 1 in 4 cancer cases in women [1]. Therefore, early diagnosis and the development of effective treatments are of vital importance. However, the search for new therapeutics in this disease is challenged by the high heterogeneity (both in clinical and molecular aspects) displayed by breast cancer. The most aggressive molecular subtype of breast cancer is the triple negative (TNBC), characterized by the lack of expression of estrogen receptor (ER), progesterone receptor (PR) and EGF receptor 2 (HER2), which is usually related with mechanisms of chemoresistance and active metastasis in patients [2].

Stauprimide, a semi-synthetic derivative of staurosporine, was characterized in 2009 as a potent enhancer of differentiation in embryonic stem cells (ESC) [3]. In that study, and despite the powerful activity of its parent compound staurosporine as a non-selective inhibitor of protein kinases (PK), the potential of stauprimide as PK inhibitor was not particularly remarkable, discarding this as the primary mode of action for the differentiation-enhancing effect reported for this molecule. Evidence about the mechanism underlying stauprimide effects in ESC pointed to the decrease of *MYC* transcription by direct interference of this molecule with nuclear translocation of NME2 [3], a *MYC* activator highly expressed in ES cells [4,5].

In addition to being involved in the maintenance of pluripotency in stem cells [6], CMYC controls the expression of a large number of genes in our organism, regulating diverse cellular processes including cell differentiation, proliferation, migration and survival, among others,

* Corresponding author at: Departamento de Biología Molecular y Bioquímica, Facultad de Ciencias, Universidad de Málaga, Andalucía Tech, E-29071 Málaga, Spain.
E-mail address: bmpoveda@uma.es (B. Martínez-Poveda).
[1] *These authors equally contributed to the paper.

https://doi.org/10.1016/j.biopha.2022.114070
Received 18 August 2022; Received in revised form 30 November 2022; Accepted 2 December 2022
Available online 14 December 2022

being considered a protoncogene [7]. Given the importance of CMYC in tumor development, the role of stauprimide in cancer was studied in a panel of different tumor cell lines *in vitro*, pointing to the possible antitumor activity of this compound [8]. In that work, the inhibitory effect of stauprimide on tumor growth was shown in an *in vivo* murine model of renal cancer, whereas its activity in other cancer types, such as breast cancer, was not described.

In this work the effect stauprimide on human TNBC cells proliferation and its underlying mechanism of action has been studied *in vitro* and the antitumor activity of this compound has been explored *in vivo* by means of orthotopic xenograft and syngeneic models. Our data show that stauprimide inhibits TNBC cells growth by a mechanism involving cell cycle arrest in G_2/M and interfering with proliferation and survival pathways without induction of apoptosis. In addition, the inhibitory effect of stauprimide in cell migration *in vitro* and the reduction of *in vivo* metastases in lung and liver indicates a role of this compound in preventing metastasis derived from TNBC. In sum, our studies point to stauprimide as a potent inhibitor of cell growth and possible antimetastatic compound in the context of TNBC.

2. Material and methods

2.1. Cell cultures and treatments

Breast carcinoma cell lines MDA-MB-231 (human, triple negative) MCF7 (human, ER+, PR+, HER2-, luminal A) and 4T1 (murine, triple negative) [9,10] were provided by ATCC (Rockville, MD, USA) and maintained in RPMI-1640 (MDA-MB-231) or DMEM containing 4.5 g/L glucose (4T1 and MCF7). Non-transformed human embryonic kidney cells (HEK-293T) and human gingival fibroblasts (HGF) were obtained from ATCC and maintained in MEM or DMEM containing 4.5 g/L glucose. All culture media were supplemented with 10 % FBS, 2 mM L-glutamine, 50 IU/mL penicillin, 0.05 mg/mL streptomycin and 1.25 mg/L amphotericin B. All cell lines were maintained at 37 °C and humidified 5 % CO_2 atmosphere. Cell culture media were purchased from Lonza (Basel, Switzerland), penicillin/streptomycin and amphotericin B were provided by BioWest (Kansas City, KS, USA), and fetal bovine serum (FBS) was purchased from Capricorn. Plastics for cell culture were supplied by Thermo Scientific Nunc (Thermo Fisher Scientific; Waltham, MA, USA). Stauprimide was purchased from Sigma-Aldrich (MERK; Darmstadt, Germany) and reconstituted in dimethyl sulfoxide (DMSO). All treatments in cells were performed in complete media at doses and times indicated in each assay; an equivalent DMSO (vehicle) dose was added in control conditions.

2.2. Methylthiazol tetrazolium (MTT) survival assay

The MTT dye reduction assay was performed as previously described [11,12]. MTT reagent was purchased from Sigma-Aldrich (MERK; Darmstadt, Germany). Briefly, 2×10^3 cells were incubated in 96-well plates in the presence of serial dilutions of stauprimide in quadruplicate. After 3 days of incubation, 10 μL of MTT (5 mg/mL in PBS) was added to each well and the plate was incubated for a further 4 h. The resulting formazan was dissolved in 0.04N HCl-2-propanol and measured in a spectrophotometer at 550 nm. IC_{50} values were calculated as the concentration of stauprimide yielding 50 % of cell growth for each cell line after 3 days of treatment. At least three independent replicates were performed of this assay.

2.3. Cell cycle analysis

Subconfluent MDA-MB-231 and 4T1 cells in 6-well plates were treated with different concentrations of stauprimide overnight. A negative control with the vehicle (DMSO) and a positive control with 20 μM 2-methoxystradiol (2-ME) were included in the assays. After treatment, cells were harvested and centrifuged. Pellets were washed with PBS supplemented with 1 % FBS and 10 mM HEPES, and then cells were fixed in 70 % ice-cold ethanol for 1 h at 4 °C. Finally, cells were centrifuged and washed twice, suspended in propidium iodide staining solution (40 μg/mL propidium iodide, 0.1 mg/mL RNase-A and 2 mM EDTA in PBS supplemented with 1 % FBS and 10 mM HEPES), and incubated for 30 min at 37 °C protected from light. Samples were analyzed in a FACS VERSE™ flow cytometer (BD Biosciences, Franklin Lakes, NJ, USA) and the percentages of cell population in G_0/G_1, S and G_2/M phases of the cycle, and the population in sub-G_1 (fragmented DNA), were determined using the BD FACSuite program (BD Biosciences). At least three independent replicates were performed of this assay.

2.4. 5-ethynyl-2′-deoxyuridine (EdU) staining and detection by flow cytometry

MDA-MB-231 cells were grown in 6-well plates (1.5×10^5 cells/well) until they reached 80 % confluence. Cells were treated overnight with different doses of stauprimide, and a negative control (cells in cultured medium containing DMSO) was included in the assay. EdU Flow Cytometry kit (BaseClick; Munich, Germany) was used in this assay. After treatments, the medium was replaced with fresh medium containing 1 μL/mL of EdU, and cells were incubated for a further 2 h. Then, cells were washed, harvested and neutralized with PBS supplemented with 1 % FBS and 10 mM HEPES. Samples were centrifuged for 5 min at 1600 rpm, washed with PSB containing 1 % BSA and fixed with 4 % PFA in PBS for 15 min in the dark. After that, cells were centrifuged and washed with 1 % BSA in PSB and permeabilized with saponin. Finally, samples were incubated for 30 min in 0.5 mL of the buffer supplied by the kit and analyzed in a FACS VERSE™ flow cytometer using the BD FACSuite program. Three independent replicates were performed of this assay.

2.5. Annexin V/7-AAD staining and detection by flow cytometry

MDA-MB-231 cells were grown in 6-well plates until subconfluence and then treated overnight with culture medium with different doses of stauprimide or DMSO (control). After treatments, cells were harvested and centrifuged for 1 min at 1600 rpm, and cell suspensions of 100000 cells/mL were prepared. The viable, necrotic, early apoptotic and late apoptosis populations were determined by the FITC Annexin-V Apoptosis Detection Kit I (BD Biosciences-Pharmingen; Franklin Lakes, NJ, USA) following the manufacturer's instructions. Samples were analyzed in a FACS VERSE™ flow cytometer using the BD FACSuite program. Three independent replicates were performed of this assay.

2.6. mRNA extraction and detection of MYC expression by real-time quantitative PCR (rt-qPCR)

Subconfluent MDA-MB-231 and MCF7 cells grown in 6-well plates were treated with different concentrations of stauprimide or DMSO (negative control) for 6 h. For total RNA isolation, cells were harvested in Tri Reagent (Merck; Darmstadt, Germany) and RNA was extracted using Direct-Zol RNA miniprep kit (Zymo Research; Irvine, CA, USA) following the manufacturer's protocol. Integrity and quantity of isolated RNA were determined in a NanoDrop One (Thermo Fisher Scientific; Waltham, MA, USA). The retrotranscription to cDNA was performed with PrimeScript™ RT Reagent Kit (Takara Bio INC.; Kusatsu, Shiga, Japan). For cDNA amplification, the SYBR Premix Ex Taq™ II (Takara Bio INC.; Kusatsu, Shiga, Japan) was used in an Eco™Real-Time PCR System (Illumina; San Diego, California, USA). Predesigned primers for qPCR analysis were used (KiCqStart™ SYBR Green Primers Predesigned; Merck-Sigma Aldrich; Darmstadt, Germany). Analysis of *MYC* expression by rt-qPCR was performed in duplicate for each sample according to the manufacturer's instructions, and at least three independent experiments were performed. All rt-qPCR data were normalized to *ACTB* gene

(β-actin) expression.

2.7. Western-blot assays

Cells were treated overnight with stauprimide at the indicated concentrations. After washing with cold PBS, protein samples were obtained in lysis buffer (0.5 M Tris-HCl, pH 6.8; 12 % SDS; 10 % glycerol). Protein concentration was measured using DC Protein Assay (Bio-Rad Laboratories; Hercules, California, USA) and β-mercaptoethanol and bromophenol blue were added at final concentrations of 5 % and 0.2 %, respectively. Samples were denaturalized at 95 °C for 5 min, and 30 μg of total protein were subjected to SDS-PAGE electrophoresis and transferred to nitrocellulose membranes. After blocking in TBS-T (Tris 20 mM, NaCl 137 mM, Tween-20 0.1 %) containing 10 % non-fatty dry milk, membranes were hybridized with primary antibodies overnight at 4 °C. Rabbit anti-Phospho-Akt (Ser473; #9271), rabbit anti-Akt (#9272), rabbit anti-phospho-p44/42 MAPK (P-ERK1/2; Thr202/Tyr204; clone D13.14.4E; #4370), rabbit anti-p44/42 MAPK (ERK1/2; 137F5; #4695), rabbit anti-phospho-p38 MAPK (Thr180/Tyr182; 12F8; #4631), rabbit anti-p38 MAPK (#9212) and mouse anti-α-tubulin (DM1A; #3873) antibodies were purchased from Cell Signaling Technology (Danvers, Massachusetts, USA). Mouse anti-$p27^{Kip1}$ (sc-1641) antibody was purchased from Santa Cruz Biotechnology (Dallas, Texas, USA) and rabbit monoclonal anti-c-MYC (Y69 clone, ab32072) antibody was purchased from Abcam (Cambride, UK). Membranes were washed in TBS-T and incubated 1 h with secondary horseradish peroxidase (HRP)-conjugated secondary antibodies at room temperature (donkey anti-rabbit IgG HRP-linked was from Merck, and horse anti-mouse IgG HRP-linked was from Cell Signaling Technology). Immunoreactive bands were detected with SuperSignal West Pico Chemiluminescent Substrate (Pierce; Rockford, USA) in a Chemidoc XRS System (Bio-Rad Laboratories; Hercules, California, USA). Densitometric quantification of the bands was performed by Fiji software [13]. The phosphorylated/total protein ratios were expressed as the percentage of the ratio phosphorylated/non-phosphorylated protein. At least three independent replicates were performed of these assays.

2.8. Cell migration assays by wound healing

Confluent cell monolayers in 6-well plates were wounded with pipet tips in two perpendicular diameters, resulting in two acellular 1 mm-wide lanes per well. Then, cells were incubated in complete medium with DMSO (positive control of migration) or medium containing different concentrations of stauprimide. Wounded areas were observed and photographed at time 0 and after 6 h of incubation with a microscope camera Nikon DS-Ri2 coupled to a Nikon Eclipse Ti microscope (Nikon, Tokyo, Japan). The migration into the cell-free area was quantified by Fiji software [13] and represented as the percentage of wounded area in the correspondent time normalized to the initial wounded area (time 0) for each experimental condition. At least three independent replicates were performed of this assay.

In order to assess the cell migration capability by time-lapse, a confluent layer of MDA-MB-231 cell in an 8-well plate was wounded using a pipette tip. Treatments and control were included in the assay in a similar manner than explained before, with additional Hoechst staining (2.5 mg/mL in PBS) in order to follow cell cycle progression for each cell. After 1 h, cells were followed by a time-lapse experiment with captures every 10 min with Leica TCS SP5 confocal microscope (20X NA 0.7). Incubation conditions of 37 °C and 5 % of CO_2 were maintained throughout the assay and individual cell tracking analysis from the borders of the scratch was monitored during cell cycle progression until the cell started the mitosis process. Image analyses were performed by Fiji Software [13], using the Manual Tracking Plugin.

2.9. Orthotopic in vivo models of TNBC (xenograft and syngeneic models)

Orthotopic xenograft breast cancer model: MDA-MB-231 cells were collected from subconfluent culture dishes (80–90 % confluence) and 1×10^6 cells in a volume of 100 μL PBS were inoculated orthotopically in the second mammary fat pad of female SCID mice (Charles River; Wilmington, Massachusetts, USA). During this procedure, animals were anaesthetized with isoflurane 1 %. For the *in vivo* studies using stauprimide, experimental groups were randomly established, and treatments were initiated 20 days after tumor cell inoculation. The design included 3 groups of animals: negative control (non-bearing tumors mice), n = 2; positive control (xenograft mice under DMSO treatment), n = 3; and stauprimide-treated xenograft mice, n = 3. Treatments were administered by oral gavage twice per week at 25 mg/Kg final concentration (approx. 20 g weight per mouse), a well tolerated dose as described in [8]. Drug administration and MRI scanning were performed for all groups for 3 weeks in total, and body weights of animals were annotated during the treatment period. Animals were sacrificed at the end of the 3 weeks of treatments, according to the animal procedures, and tumors, lungs, kidneys and livers were processed for histology.

Orthotopic syngeneic breast cancer metastasis model: 4T1 murine TNBC cells (1×10^6 cells in a volume of 100 μL PBS) were inoculated orthotopically in the second mammary fat pad of 9 weeks old BALB/c female mice. 3 days after inoculation of cells, two experimental groups were randomly established and animals were treated with vehicle (DMSO; n = 5) or stauprimide (25 mg/kg; n = 4) twice per week. The progression of the tumoral masses was followed by MRI, and body weights of animals were annotated during the experiment. After 21 days, mice were sacrificed according to the animal procedures, and tumors, lungs and livers were processed for histology.

All the MRI experiments were carried out on a 9.4 T Bruker Biospec System equipped with 400 mT/m gradients. All studies were conducted on a 40 mm quadrature bird-cage resonator. High resolution T2-weighted images were acquired using a turbo-RARE sequence with respiratory gating (TE = 16 ms, TR = 1000 ms, 4 averages, 156 μm in-plane resolution and 1 mm slice thickness).

These experiments were performed in accordance with the Spanish and European Guidelines for Care and Use of Laboratory Animals (R.D. 53/2013 and 2010/62/UE) and approved by our Local Animal Ethics Committee, and the Highest Institutional Ethical Committee (Andalusian Government, accreditation number 14/09/2021/129).

2.10. Histologic samples preparation and processing

Tissues were fixed in 4 % formaldehyde (pH 7 buffered; Panreac Química, Castellar del Vallès, Barcelona, Spain) for 48 h, changing the 4 % formaldehyde after 24 h. Then, samples were dehydrated through graded ethanol, and embedded in paraffin (temperature 56 °C for 2 h under stirring and vacuum). All procedures were performed following the same steps: paraffin-embedded samples were sectioned at 6 μm thickness, then deparaffinized (2 steps of 10 min in xylol) and rehydrated (2 steps of 5 min in absolute ethanol, 2 steps of 5 min in 96 % ethanol, 5 min in 70 % ethanol and 5 min in distilled water). Then, tissue sections were stained with different protocols.

Hematoxylin and Eosin (H&E) staining: Sections were incubated for 5 min in Harris Hematoxylin solution, 5 min in 96 % ethanol and 5 min in distilled water. Then, sections were rinsed in 96 % ethanol and finally incubated 3 min in 1 % of Eosin Yellowish hydroalcoholic solution.

Immunohistochemical detection of Ki67: It was performed following the manufacturer indications of VitroView In Situ Ki67 IHC-DAB Detection Kit (VitroVivo Biotech, Maryland, USA). Quantification of Ki67-positive cells and the total number of cells in tissue sections was performed in random areas of the tumors, using Fiji software [13] and following the method described in [14].

May-Grünwald-Giemsa: Blood was drawn from the tail of the mouse. A blood smear was made on a slide using a freshly drawn drop. Then,

samples were dried at room temperature. At this point, samples were stained with May-Grünwald's eosin-methylene blue solution modified for 5 min and Giemsa's Azure Eosin Methylene Blue solution (1:7) in PBS for 15 min. Finally, samples were dried at room temperature and mounted on commercial glass slides.

2.11. Statistical analysis

Quantitative results are expressed as means ± SD of at least three independent experiments. Statistical significance was determined using GraphPad Prism software by two-sided unpaired Student's t-test or ANOVA, and values of $p < 0.05$ were considered to be statistically significant. p-values were represented as: *$p < 0.05$; **$p < 0.01$; ***$p < 0.001$.

3. Results

3.1. Stauprimide affects cell growth and survival in breast cancer cell lines

As a first approximation to evaluate the effect of stauprimide (Fig. 1A) in breast cancer cell lines, MDA-MB-231 (human, triple negative), 4T1 (murine, triple negative) and MCF7 (human, ER+, PR+, HER2-, luminal A) cells were grown for 3 days in the presence of increasing doses of this compound. Cell viability was then evaluated by the MTT assay and survival curves revealed that, although stauprimide reduced cell growth in the three cell lines, the inhibitory effect was more pronounced in the case of MDA-MB-231 (IC_{50} 1.07 ± 0.52 μM) and 4T1 (IC_{50} 0.8 ± 0.1 μM) cells compared to MCF7 (IC_{50} >20 μM) (Fig. 1B, Suppl. Fig. 1). Interestingly, in non-transformed cell lines HEK-293 T (human embryonic kidney cells) and HGF (human gingival fibroblasts) stauprimide exhibited low toxicity, since IC_{50} values were at least one order of magnitude higher than the calculated for TNBC cells (Fig. 1B and Suppl. Fig. 1).

The observation of the stronger effect exhibited by stauprimide in MDA-MB-231 and 4T1 cells compared to MCF7 and non-transformed cell lines led us to further explore the anticancer role of stauprimide in TNBC cells. A possible cytostatic effect of the compound was derived from the survival curve obtained for MDA-MB-231 cells, since despite its low IC_{50} value the curve did not reach 100 % of mortality. However, this effect was less marked in 4T1 cells, in which the survival drops near to zero (Fig. 1B and Suppl. Fig. 1).

The cell growth of MDA-MB-231 was monitored along 6 days in presence of different concentrations of stauprimide, observing a significant reduction in cell growth from day 2 compared to control for all the treatment conditions (Fig. 1C). Of note, at the dose of 0.5 μM of stauprimide, after a slight increase during the first 2 days, cell number remained almost invariant until the end of the experiment. Higher doses of stauprimide (2 and 10 μM) exhibited a stronger inhibition of cell growth from day 2, but they did not induce total cell death after 6 days, supporting the effect observed in survival curves and suggesting an impairment in cell proliferation rather than a direct toxicity effect in this cell line.

3.2. Stauprimide induces cell cycle arrest and inhibits proliferation in MDA-MB-231

In view of the observed effects of stauprimide in survival and cell growth of MDA-MB-231 cells, the influence of the compound on cell cycle progression was studied. After treatment with different doses of stauprimide (0.5, 2 and 10 μM) for 16 h in MDA-MB-231 cells, IP staining was performed and cell cycle analysis was carried out, showing a clear reduction of cell population in G_0/G_1 phase in parallel with an evident increase of cell population in G_2/M phases in 10 μM stauprimide-treated cells (Fig. 1D,E). These data indicated that the compound clearly induced cell cycle arrest in G_2/M in MDA-MB-231, a similar effect to the observed changes induced by 2-methoxyestradiol (2-ME), used as positive control of cell cycle blockage.

According to the possible effect of stauprimide on cell proliferation suggested by the results obtained in cell growth curves and cell cycle analysis, EdU incorporation was measured in MDA-MB-231 cells in presence of different doses of the compound. As shown in Fig. 2A,B, stauprimide reduced the proportion of cells that incorporated EdU (proliferative cells) compared with untreated cells, increasing at the same time the proportion of quiescent cells (Fig. 2B). These results suggested that the compound inhibited cell proliferation in a direct manner.

Interestingly, in cell cycle analysis, no significant increase in cells with fragmented DNA ($subG_1$) was observed with treatments (Fig. 1E), suggesting that stauprimide may not be inducing apoptosis in MDA-MB-231 cells under the assayed conditions. To corroborate this observation, the exposition of annexin-V in the cell membrane of MDA-MB-231 in absence (negative control) and presence of stauprimide was studied. Analysis of the data showed that stauprimide neither increased the population of cells in early apoptosis (annexin-V positive, 7-AAV negative) nor the proportion of cells in late apoptosis (annexin-V positive, 7-AAV positive) (Fig. 2 C,D), indicating the absence of apoptosis induction under these treatment conditions. Interestingly, the population of death cells (annexin-V negative, 7-AAD positive) was not higher in treated cells compared to the control (Fig. 2D), suggesting a low toxicity of stauprimide in MDA-MB-231 cells. However, despite apoptosis was not detected in MDA-MB-231 cells treated with stauprimide, in 4T1 murine TNBC cells this compound increased the population of cells in $subG_1$ compared to control condition, indicating a possible apoptosis induction in 4T1 in response to stauprimide (Suppl. Fig. 2).

3.3. Stauprimide modulates growth and survival signalling pathways in breast cancer cells, and inhibits MYC expression

To get a deeper insight into the molecular mechanism of stauprimide underlying the observed effects on MDA-MB-231 growth and survival, the possible influence of this compound on proliferation and survival signalling pathways was investigated. Results showed that stauprimide significantly inhibited the PI3K/Akt survival pathway in a dose-response manner in MDA-MB-231 (Fig. 3A,B), together with the reduction in the MAPK-ERK1/2 pathway (Fig. 3C,D). In addition, the MAPK-p38 pathway was increased in presence of stauprimide (Fig. 3E,F), indicating a modulatory pattern of this compound in the main signalling axis related to cell growth and survival.

According to IC_{50} values, stauprimide did not affect MCF7 cells so strongly compared to MDA-MB-231 and 4T1 TNBC cells (Fig. 1B). In order to determine if the different behaviour of the breast cancer cell lines was due to a differential effect of stauprimide in modulation of signalling pathways, the activation of PI3K/Akt, ERK1/2 and p38-MAPK pathways was analyzed in MCF7 cells. Interestingly, in contrast with the effect detected in MDA-MB-231 cells (Fig. 3A,B), stauprimide significantly increased the phosphorylation of Akt in MCF7 cells (Suppl. Fig. 3A,B), denoting a differential modulation of the pathway. However, stauprimide decreased the activation of ERK1/2 pathway (Suppl. Fig. 3D,E) and increased phosphorylation of p38-MAPK (Suppl. Fig. 3F,G) in MCF7 cells, similar to the effects detected for stauprimide in MDA-MB-231 (Fig. 3C-F). These data suggest that activation of PI3K/Akt survival pathway in stauprimide-treated MCF7 cells could be buffering the antiproliferative effect of the compound, in contrast with the more pronounced effect achieved in MDA-MB-231, where PI3K/Akt pathway was downregulated by stauprimide.

In addition to the observed effect in signalling pathways, we analysed the level of CMYC (a key regulator of cell cycle progression [15]) in MDA-MB-231 and in MCF7 in presence of stauprimide, since *MYC* downregulation was proposed as the main mechanism of action of stauprimide priming differentiation in embryonic stem cells and targeting renal cancer cells [3,8]. As shown in Fig. 3 G,H, treatment with stauprimide in MDA-MB-231 cells reduced CMYC in a dose-dependent

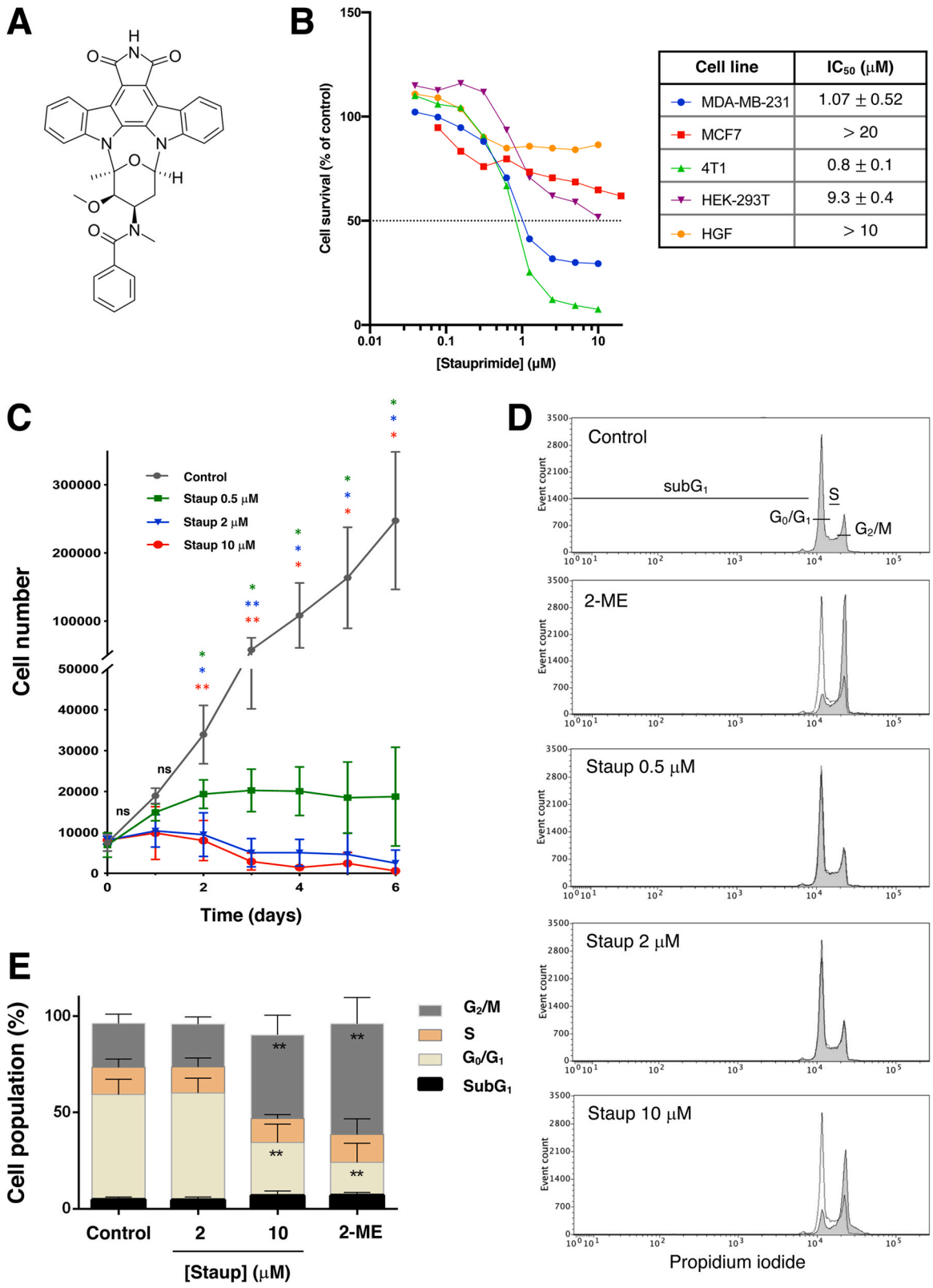

Fig. 1. Studies of cell survival in different cell lines, and analysis of cell cycle in MDA-MB-231. (A) Molecular structure of stauprimide. (B) Survival curves and IC_{50} values of different breast cancer and non-transformed cell lines in presence of stauprimide for 72 h (means of 3 independent experiments are showed). (C) Growth curves of MDA-MB-231 cells in presence of different doses of stauprimide (staup) for 6 days. (D) Cell cycle representative profiles of IP-stained MDA-MB-231 cells in different experimental conditions; 2-ME (2-methoxyestradiol) 20 μM was used as positive control; the unfilled overlaid curve represents the DMSO control (E) Quantitative data of cell cycle analysis in MDA-MB-231 cells in absence or presence of stauprimide. In C and E, data represented mean + /- S.D. of 3 independent experiments. Statistical analysis in C was performed by two-way ANOVA-multiple comparisons, and two-sided unpaired Student's t-test was used in E; D is a representative profile of 3 independent experiments.

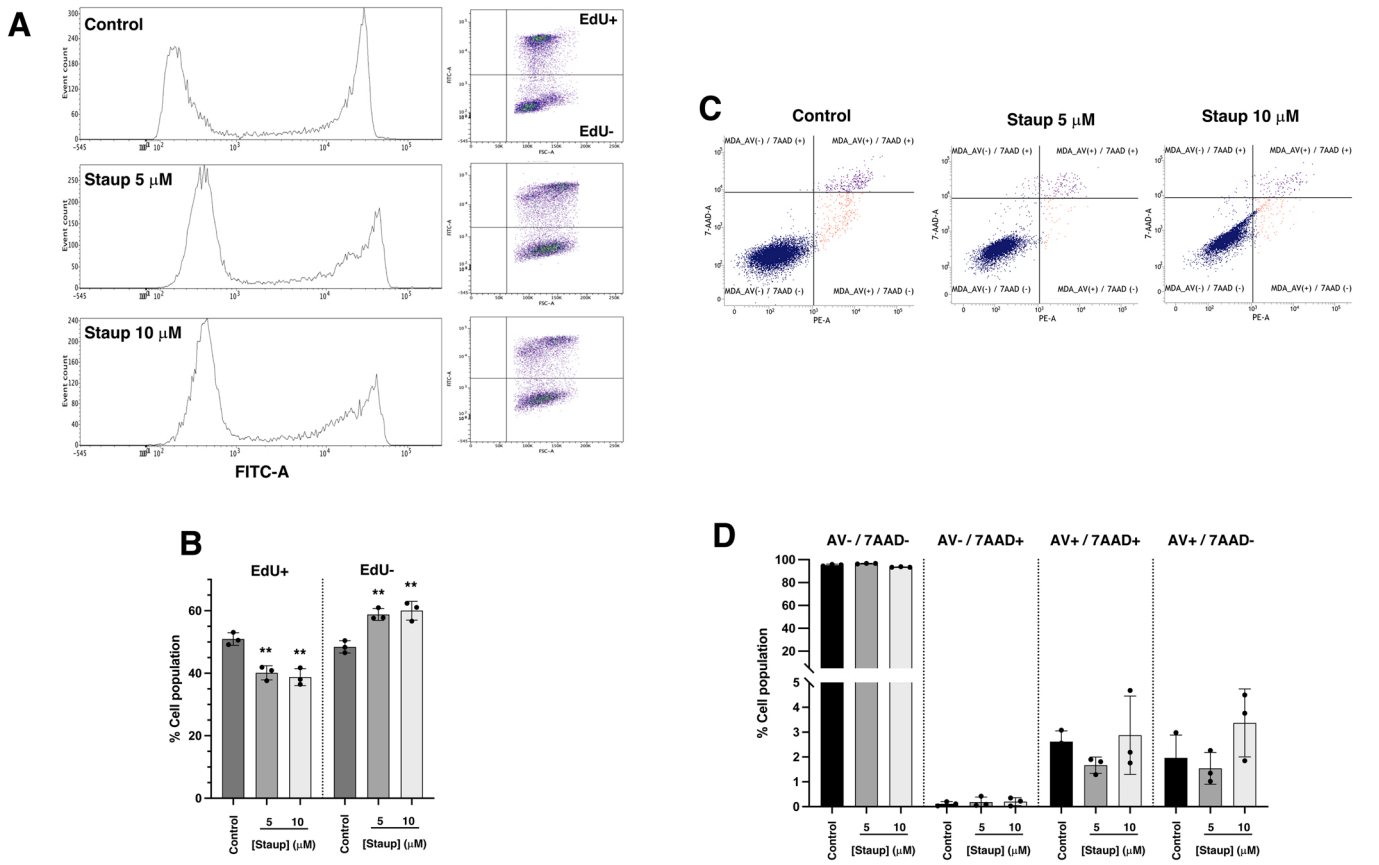

Fig. 2. Proliferation assay by EdU and study of annexin-V exposition in MDA-MB-231. (A) Flow cytometry representative profiles of EdU-treated MDA-MB-231 cells in absence (control) or presence of stauprimide at different doses. (B) Quantitative data of EdU analysis in MDA-MB-231 subjected to different experimental conditions. (C) Representative profiles of annexin-V assay in MDA-MB-231 in absence (control) or presence of stauprimide. (D) Quantitative data of annexin-V assay in MDA-MB-231; AV-/7AAD- (cell population negative for both annexin-V and 7AAD, non-apoptotic cells), AV-/7AAD+ (cell population negative for annexin-V and positive for 7AAD, death cells), AV+ /7AAD+ (cell population positive for both annexin-V and 7AAD, cells in late apoptosis), AV+ /7AAD- (cell population positive for annexin-V and negative for 7AAD, cells in early apoptosis). In B and D, data represented mean +/- S.D. of 3 independent experiments and statistical analysis was performed by two-sided unpaired Student's t-test; A and C are representative profiles of 3 independent experiments in each case.

manner, correlating with a lower mRNA level (Fig. 3I), suggesting the involvement of CMYC reduction in the observed effects of the compound in these cells. In parallel, the expression of *MYC* was decreased in MCF7, but the reduction did not reach even the 50 % (Suppl. Fig. 3G), in contrast to the 60 % inhibition detected in MDA-MB-231 (Fig. 3I), and it did not follow a dose-response pattern (Suppl. Fig. 3G). No differences were detected in the level of CMYC mRNA between the two cell lines (Suppl. Fig. 3H).

Finally, we measured the presence of $p27^{Kip1}$ in MDA-MB-231 cells treated with stauprimide, since it was reported that CMYC induced a direct downregulation of this cyclin-dependent kinase inhibitor in breast cancer cells [16]. However, the level of $p27^{Kip1}$ in MDA-MB-231 cells was unaffected in presence of stauprimide at the used experimental conditions (Suppl. Fig. 4A,B).

3.4. Stauprimide affects migratory potential of MDA-MB-231

In addition to the inhibitory role of stauprimide in cell proliferation, the capability of this compound to interfere in the migratory potential of MDA-MB-231 was explored. Wound-healing assays showed a significant reduction in the migration of these cells after 6 h of treatment with 2 and 10 μM of stauprimide (Fig. 4A,B). Additionally, time-lapse microscopy was performed in order to observe in detail the response of the cells to the treatment. Cells were followed from 1 h to 8 h from the initial treatment (Fig. 4C and Suppl. Movies 1–4), and quantitative parameters of migration velocities and distances were measured in the different conditions. As shown in Fig. 4D,E, the motility of cells was compromised in presence of stauprimide, showing a significant reduction of migration distances and velocities at 2 and 10 μM doses. In addition, at the highest dose of stauprimide, cell morphology was clearly affected, showing a rounded shape without cell extensions. Importantly, according to the follow-up of Hoechst-stained cell nuclei throughout the assays, cell proliferation was not detected at the analysed time points (data not shown).

Supplementary material related to this article can be found online at doi:10.1016/j.biopha.2022.114070.

Supplementary material related to this article can be found online at doi:10.1016/j.biopha.2022.114070.
Supplementary material related to this article can be found online at doi:10.1016/j.biopha.2022.114070.
Supplementary material related to this article can be found online at doi:10.1016/j.biopha.2022.114070.

3.5. Stauprimide affects breast cancer progression and metastasis in vivo

In view of the results obtained in MDA-MB-231 *in vitro*, the *in vivo* effect of stauprimide was explored in an orthotopic xenograft model of breast cancer. After MDA-MB-231 inoculation in the mammary gland of SCID female mice, tumor growth was followed by MRI. On day 20, when tumoral masses reached measurable dimensions, stauprimide treatment was initiated, and the evolution of tumor growth was followed by MRI images in the experimental groups (Fig. 5A), together with a recording

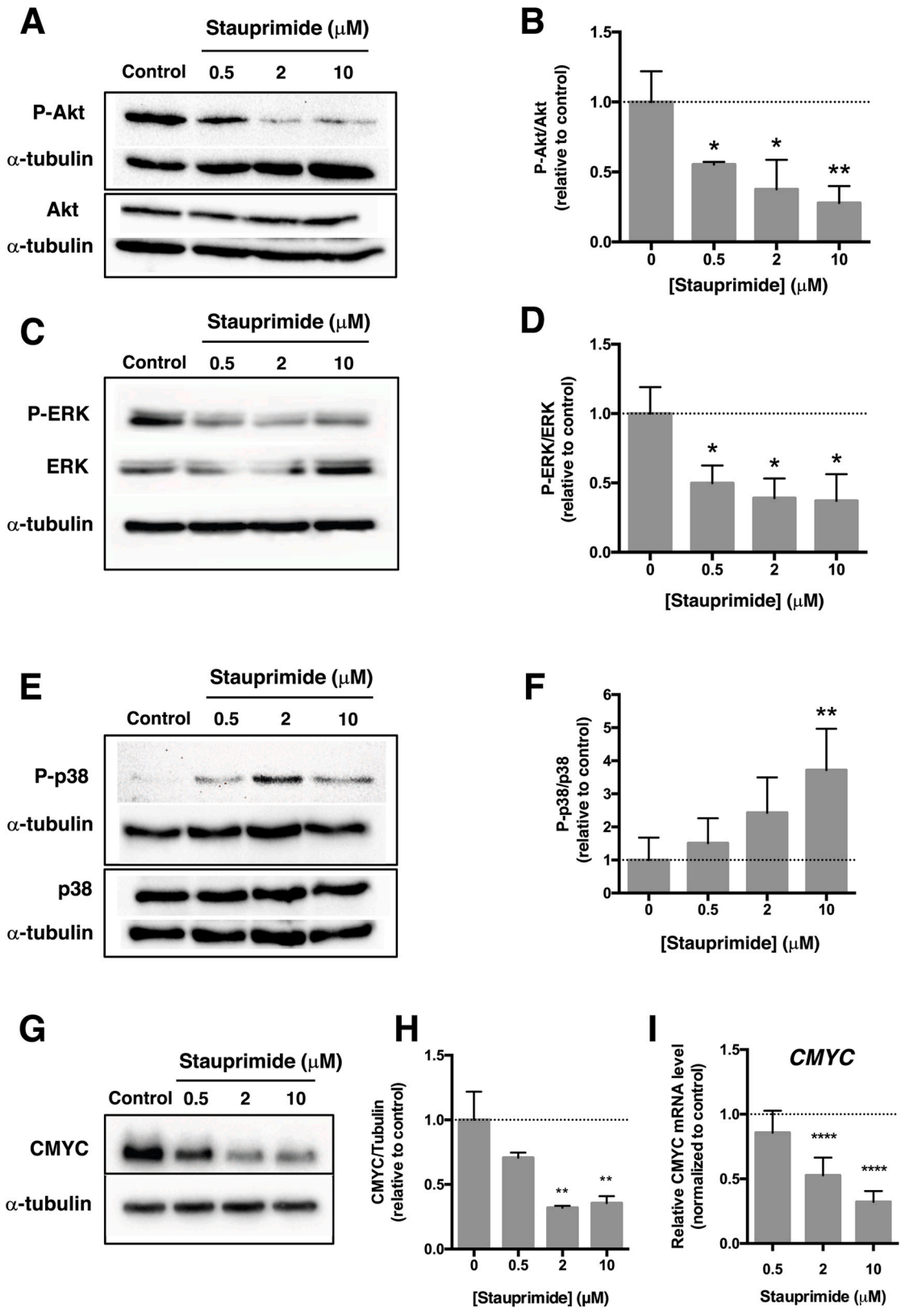

Fig. 3. Study of signalling pathways and CMYC expression in MDA-MB-231 cells. Representative Western-blots of (A) phospho-Akt (P-Akt), total Akt, (C) phospho-ERK (P-ERK), total ERK, (E) phospho-p38 (P-p38), total p38, and α-tubulin in MDA-MB-231 in absence (control) or presence of stauprimide for 16 h. (B, D, F) Quantitative data of densitometric analysis of Western-blots in A, C and E. (G) Representative Western-blots of CMYC and α-tubulin in MDA-MB-231 in absence (control) or presence of stauprimide for 16 h. (H) Quantitative data of densitometric analysis of Western-blots in G, representing CMYC signal relative to α-tubulin. (I) Relative *MYC* mRNA expression in MDA-MB-231 treated with stauprimide during 16 h; data were normalized with *ACTB* (β-actin) mRNA expression for each condition and normalized to control condition. In B, D, F, H and I, data represented mean +/- S.D. of 3 independent experiments and statistical analysis was performed by two-sided unpaired Student's t-test; A, C, E and G are representative results of 3 independent experiments in each case.

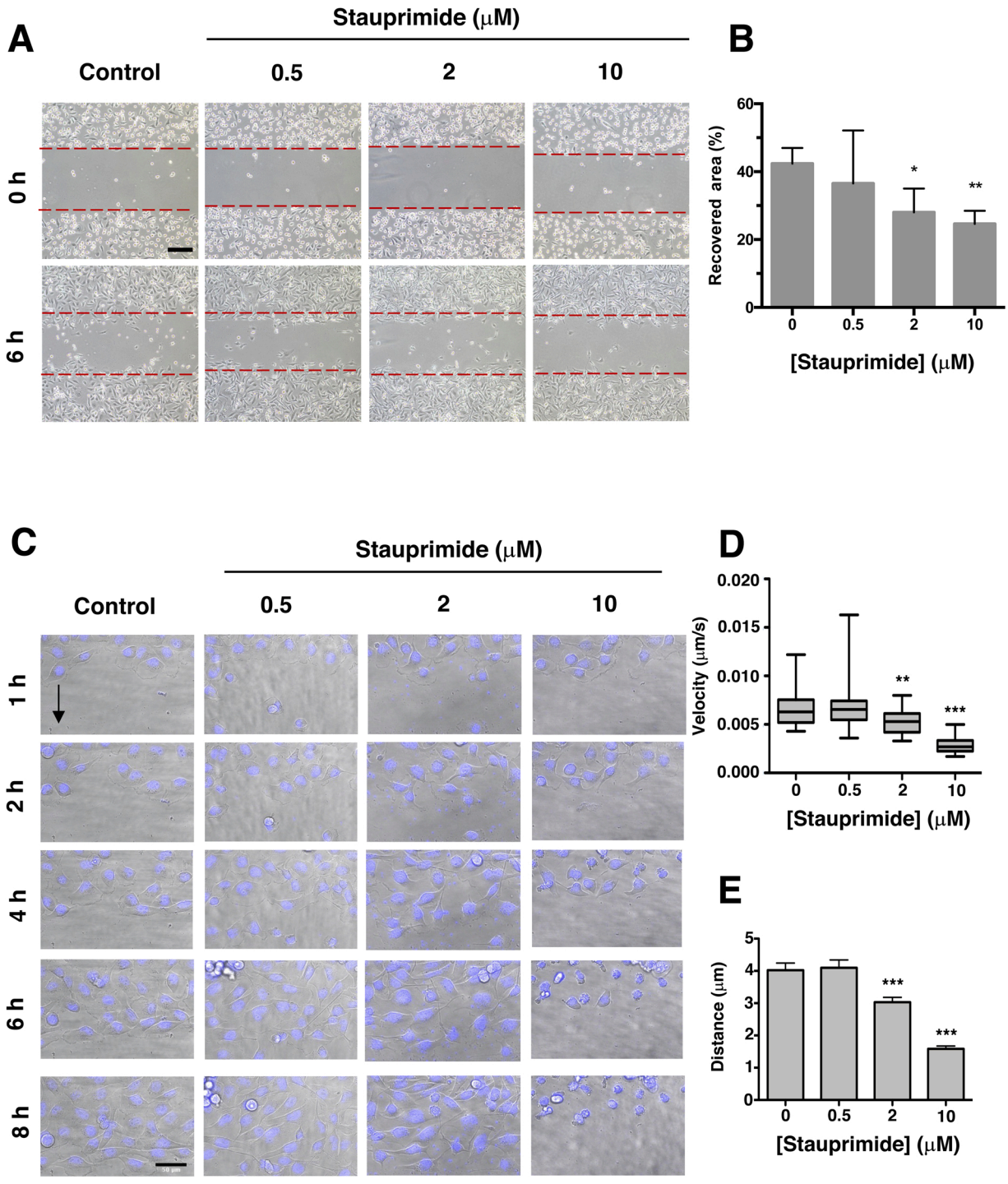

Fig. 4. Migration assays in MDA-MB-231 cells. (A) Representative images of wound-healing assay of MDA-MB-231 in absence (control) or presence of stauprimide at time zero and after 6 h of treatment; red lines denote the initial wound in each case; error bar: 500 μm. (B) Quantitative analysis of recovered area in wound-healing assay after 6 h; data represented mean + /- S.D. of 3 independent experiments and statistical analysis was performed by two-sided unpaired Student's t-test. (C) Representative images of wound-healing assay performed in MDA-MB-231 with time-lapse microscopy in absence (control) or presence of stauprimide; different time-points are showed of a followed representative area in each condition; black arrow denotes the direction of migration; cells were stained with Hoechst; error bar: 50 μm. (D) Quantitative analysis of cell velocity (μm/s) and (E) covered distance (μm) measured for different individual cells in time-lapse wound-healing assays performed in absence or presence of stauprimide. Time-lapse microscopy was performed twice with similar results. Statistical analysis was performed by two-sided unpaired Student's t-test.

of the animal weights during the assay (Suppl. Fig. 5A). Tumor volume was calculated from MRI measurements as described in the Materials and Methods section and normalized to the initial volume of each tumor at the starting of the treatments, revealing a similar growth of both DMSO- and stauprimide-treated mice from day 20 until day 27 (Fig. 5B). From this day, tumors of stauprimide-treated mice showed a slight but significant reduction in relative volume compared to the DMSO group (Fig. 5B). In addition, the growth rate of tumors in both groups was calculated, suggesting a decrease in the case of stauprimide-treated mice, as denoted by the slope values reached in each group (Fig. 5C).

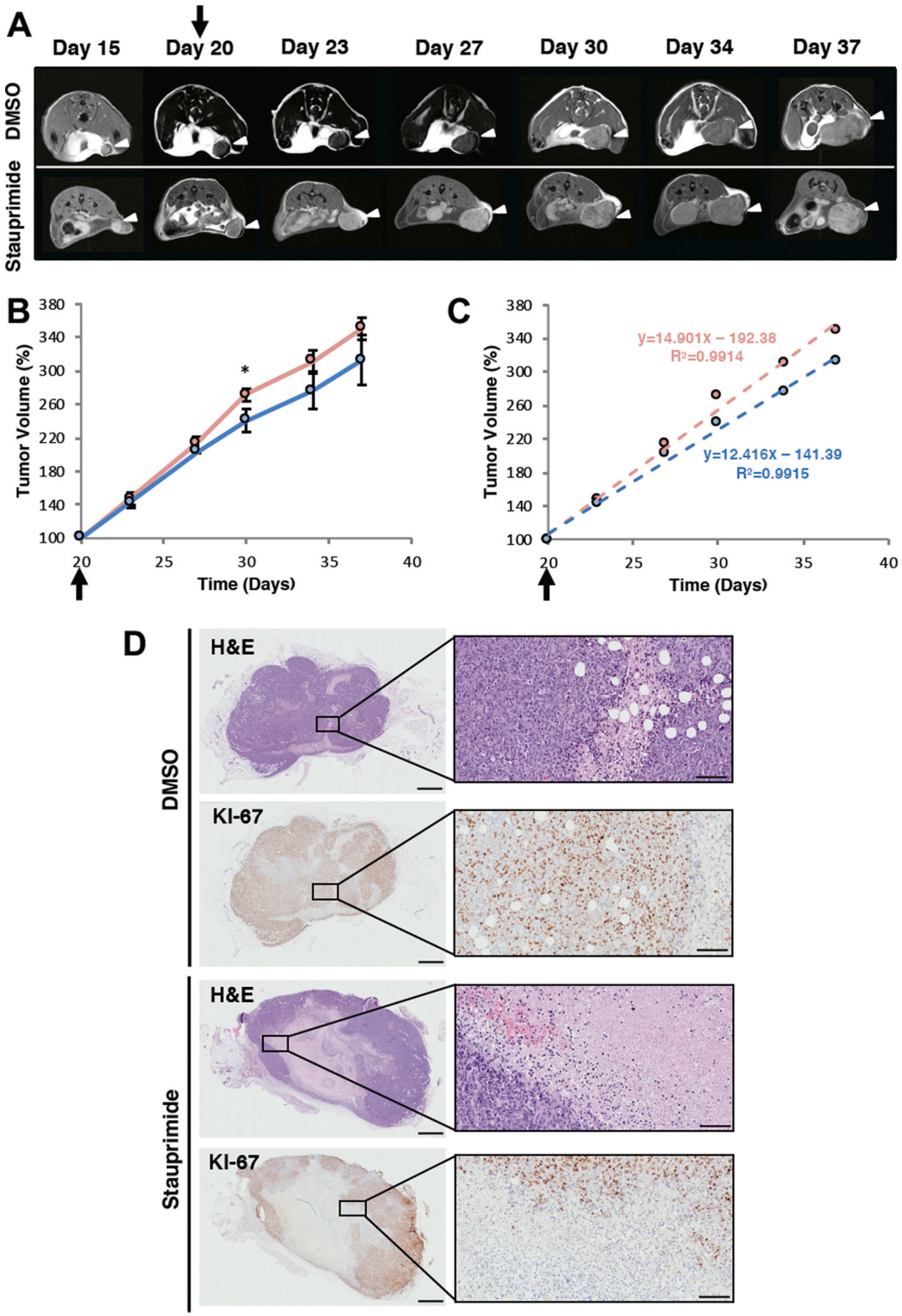

Fig. 5. In vivo assay of MDA-MB-231 orthotopic xenograft model. (A) Representative cross-sectional MRI images of MDA-MB-231 tumors (white arrowheads) developed in an orthotopic model in SCID mice; stauprimide or vehicle (DMSO) treatments were initiated at day 20 (black arrow) and repeated twice a week; tumors were followed by MRI until day 37. (B) Quantitative analysis of tumor volumes measured by MRI in DMSO (red line) and stauprimide-treated (blue line) mice; tumor volumes were normalized to volume at the start of treatments in each animal and Sutudent's t-test analysis was performed to compare tumor-volume progression in both groups; black arrow denotes the start of the treatments. (C) Linear regression analysis of data represented in B. (D) Left, representative H&E staining and Ki-67 IHC of breast tumors in DMSO and stauprimide-treated animals, scale bars: 1000 μm. Right, delimited for black box, high-magnification areas from equivalent regions in left images, scale bars: 100 μm. In each experimental group, n = 3 mice.

Although a strong effect of stauprimide in tumor growth was not evidenced, histological processing by H&E staining revealed that tumors from stauprimide-treated mice showed a heterogeneous cell density distribution pattern, with a large necrotic core, and proliferative cells (Ki67+) restricted to the most external areas (Fig. 5D). In contrast, tumors of the DMSO group were more homogeneous in cell density, and proliferative cells (Ki67+) were distributed along the whole tumoral area (Fig. 5D). However, quantitative analysis of Ki67 + cells of tumors from stauprimide-treated mice compared to tumors from DMSO-treated mice indicated that the percentage of Ki67 + cells in proliferative areas was similar in both experimental groups (Suppl. Fig. 5B).

In order to evaluate the role of stauprimide in metastasis, we studied different susceptible organs, such as liver, kidney and lung, in the experimental groups. H&E staining in these tissues showed the absence of micrometastases in all the conditions, evidencing the lack of metastasis formation during the assay (Suppl. Fig. 6 A). Nevertheless, May-Grünwald-Giemsa staining of blood samples showed that the percentage of white blood cells in DMSO-treated tumor-bearing mice was increased compared to the non-tumor bearing control group (animals without cancer cells injection) (Suppl. Fig. 6B,C), probably denoting the activation of an tumor-associated immune response in the animals. Interestingly, in the stauprimide-treated tumor-bearing mice, the percentage of white blood cells was similar to that measured in the control group (Suppl. Fig. 6B,C).

Given that no distant organ metastasis were detected in the MDA-MB-231 orthotopic xenograft model, a syngeneic orthotopic model of breast cancer with 4T1 cells (murine TNBC) was performed in immunocompetent BALB/c mice. This model represent a more standardized system in which orthotopic injection of cells derives in efficient metastasis in lungs, liver, and other tissues [17], compared to the poorly metastatic ability of MDA-MB-231 *in vivo* when inoculated orthotopically [18].

During the assay, the progression of the tumoral mass was followed by MRI. The growth of 4T1 tumors was faster than the detected in MDA-MB-231 xenograft, and data did not reveal a decrease in growth rate in stauprimide-treated animals compared to DMSO-treated mice (Suppl. Fig. 7A). In parallel to treatments, body weights of mice were followed, revealing a significant reduction in body weight in DMSO-treated mice compared to stauprimide-treated group, in which animals remain in constant body weight during the assay (Suppl. Fig. 7B). Despite the lack of reduction in tumor growth in stauprimide-treated mice, histological analysis indicated a clear increase in necrotic areas inside the tumors of this group, as was detected for MDA-MB-231 tumors. In addition, cell density in tumors of stauprimide-treated animals was lower compared to tumors in DMSO-group.

As it was expected, at the end of the experiment animals developed metastases in lungs and liver (Fig. 6A,B). As shown in Fig. 6A, lungs of DMSO-treated mice showed metastatic proliferative nodules, as denoted by Ki67 + stainning. In stauprimide-group, these proliferative masses were not detected, indicating a reduction in metastasis in this organ. In addition, livers of DMSO-group showed a high number of micrometastatic nodules, and stauprimide treatment significantly reduced the number of micrometastases in the liver of the animals (Fig. 6B,C).

4. Discussion

The alarming rates of breast cancer incidence today make it necessary the search for new therapies and drugs in order to address the current situation. In this context, data shown in this work on the effect of stauprimide reveal the potential of this compound to reduce the proliferation of human triple-negative breast cancer (TNBC) cells *in vitro*, also affecting their migratory capability. Accordingly, *in vivo* data obtained from a murine model of orthotopic xenograft provide evidence of an increase in the necrotic areas of stauprimide-treated animals, which could compromise the integrity of tumors and underly an antitumoral potential of stauprimide in breast cancer.

In this work, we evidenced that the small molecule stauprimide exerted a potent inhibition of proliferation in the TNBC cell lines MDA-MB-231 and 4T1, denoted by the reduction in cell survival and growth curves, and also observed in the decrease in EdU labelled cells as a consequence of a reduced DNA synthesis. Interestingly, the IC_{50} values obtained for MDA-MB-231 (1.07 μM) and 4T1 (0.8 μM) were similar to the reported data for renal cancer cell line RXF 393 (780 ± 160 nM) [8], being more than an order of magnitude lower than that obtained for MCF7, an ER+ , PR+ , HER- luminal-A breast cancer cell line (IC_{50} higher than 20 μM), and for non-transformed cell lines (HEK-293 and HGF). This suggests a stronger effect of stauprimide in TNBC, a high aggressive subtype of breast cancer defined by a high proliferative potential and uncontrolled growth, in addition to the lack of response to antitumoral agents [2]. Despite the clear reduction in cell proliferation observed *in vitro* in MDA-MB-231 cell line, breast tumors developed in an orthotopic xenograft model showed a slight decrease in growth rate when animals were treated with stauprimide, although a clear increase of the necrotic area inside the tumors was observed. This effect of stauprimide increasing the necrotic area of tumors was also detected in the 4T1 orthotopic syngeneic model, although in this case, the growth rate of the tumors was unaffected by the compound. It is important to note that, even when the necrotic core was increased, the external area of the tumors presented a similar Ki67 + staining, contributing to tumor growth. The anticancer effect of stauprimide was firstly described in a renal cancer model [8], and now our data point to an effective antitumoral effect of this compound in TNBC, promoting necrosis of the tumors.

Mechanistically, in this work we revealed a strong cell cycle arrest in G_2/M phase of MDA-MB-231 cells in presence of stauprimide, indicating a clear blockage of cycle progression, which results in an impairment of cell proliferation. Although we did not observe signs of apoptosis induction in MDA-MB-231 in the assayed conditions, it has been well documented that prolonged mitotic arrest in cells should result in activation of apoptosis or, in a certain genetic context, drive the cells into a senescence-like phenotype [19]. In view of the growth curves of MDA-MB-231, stauprimide seems to be exerting a cytostatic effect in these cells, only decreasing cell survival at long-term points. This would fit with the mentioned senescence-like phenotype that courses with prolonged mitotic arrest, which would represent an antioncogenic strategy [19,20]. However, stauprimide increased the population of cells with fragmented DNA ($subG_1$) in 4T1 cells, probably indicating that in these murine cells the compound exhibits stronger effect in cell viability, even inducing apoptosis at high doses. This observation would explain the sharper decrease in cell survival observed in 4T1 compared to MDA-MB-231 in presence of stauprimide.

After exploration of the activation state of some of the main pathways implicated in cell growth and survival, we found that stauprimide reduced the activation of ERK1/2 MAPK and PI3K/Akt in MDA-MB-231 cells. Interestingly, Zhu and collaborators showed that stauprimide at low doses (0.5 μM) exhibited a poor ability to inhibit kinase proteins in a non-cellular based *in vitro* system [3], in contrast with the potent multikinase inhibitory activity of its parent natural compound staurosporine. However, in those experiments stauprimide showed a consistent inhibition on certain kinases, such as Mixed-Lineage Kinase 1 (MLK1, 55 % inhibition at 0.5 μM of stauprimide). MLK1 (also known as MAP3K9 or MEKK9) is a protein kinase involved in signal transduction that is frequently expressed in certain cancer types, as is the case of melanoma and breast cancer [21,22] and is located upstream of different signalling axes such as ERK1/2 MAPK, among others [23]. Consistent with the formerly described inhibition of MLK1, our data show that stauprimide reduced the activation of ERK1/2 MAPK in MDA-MB-231. Since the MEK1/ERK1/2 pathway is known to be involved in cell proliferation mainly in response to mitogens, and its overactivation in many human tumors has been documented [23], its inhibition in MDA-MB-231 cells in response to stauprimide could contribute to the observed impairment in proliferation in these cells. In

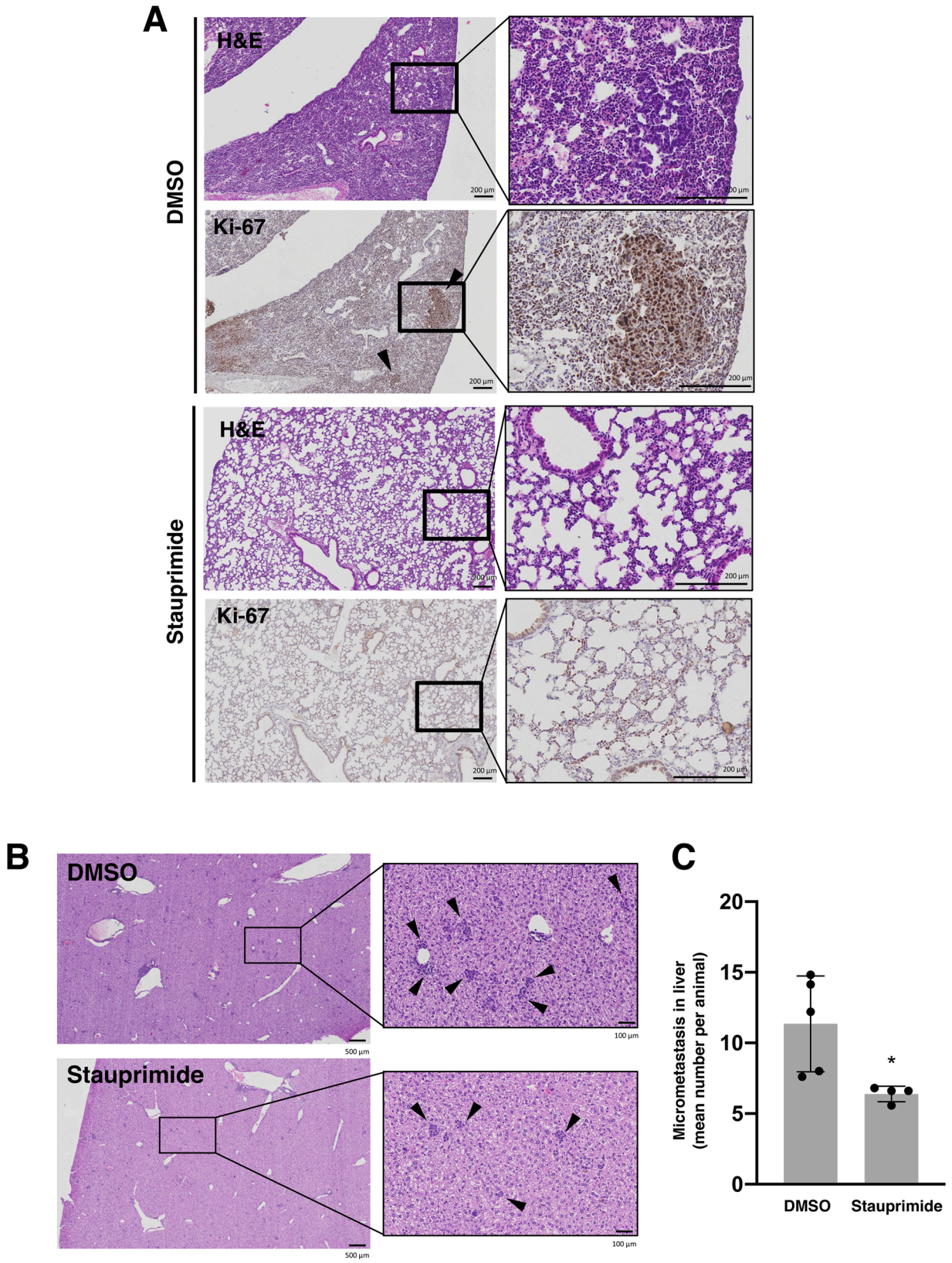

Fig. 6. Study of metastasis in lungs and livers of 4T1 orthotopic syngeneic model. (A) H&E staining and Ki67 detection in lung tissue of DMSO- and stauprimide-treated mice; arrowheads point to proliferative metastasis; error bars: 200 µm. (B) H&E staining in liver tissue of DMSO- and stauprimide-treated mice; arrowheads point to micrometastatic nodules; error bars in left panels: 500 µm; error bars in insets: 100 µm. (C) quantification of micrometastases in livers of DMSO- and stauprimide-treated mice; graft shows mean number of micrometastases quantified in 5 random areas of liver tissue for each animal (n = 5 for DMSO group, n = 4 for stauprimide group); statistical analysis was performed by two-sided unpaired Student's t-test.

parallel, in this work we describe that stauprimide inhibits Akt phosphorylation in MDA-MB-231 cells. The PI3K/Akt signalling pathway controls normal cellular processes such as cell proliferation, growth, survival and motility. These processes are critical for tumorigenesis and consequently, an aberrant activation of the PI3K/Akt axis has been observed in many cancers, including TNBC [24–26]. The reduction in Akt phosphorylation, together with ERK1/2 MAPK downregulation, in presence of stauprimide would fit with the observed decrease in proliferation in MDA-MB-231. In view of our data, we discarded a multitarget kinase inhibitory effect as the underlying mechanism of action of stauprimide in the modulation of proliferation, since this compound reduced cell growth of MDA-MB-231 and inhibited PI3K/Akt and ERK 1/2 signaling pathways at low dose (0.5 μM), in which a multikinase inhibitory ability of the compound was not detected, as reported in [27].

Despite the role of PI3K/Akt pathway in survival mainteinance in cells, we did not observe apoptosis induction in stauprimide-treated MDA-MB-231 cells, probably due to the activation of multiple pathways implicated in cell survival and the dysregulation on apoptotic machinery described in TNBC, which allow evasion of apoptosis [28,29]. Moreover, in accordance with the downregulation observed in PI3K/Akt pathway, the migratory potential of MDA-MB-231 cells is compromised in presence of stauprimide, suggesting a possible anti-metastatic effect of this compound in breast cancer tumors. Although we did not detect the presence of micrometastatic nodules in the analysed tissues derived from animals of the MDA-MB-231 orthotopic model, our data suggested a reduced presence of white blood cells in circulating blood of stauprimide-treated tumor-bearing mice compared to DMSO group, which could indicate the absence of a tumor-elicited pro-inflammatory environment in the stauprimide-treated animals, a process related to the initiation of metastasis from the primary tumor [30–32]. Complementarily, in the 4T1 orthotopic syngeneic model used in this work, we detected a reduction in metastases in lungs and livers of animals treated with stauprimide, pointing to the anti-metastatic potential of this compound. Of note, animals in DMSO-group exhibited a significant reduction in body weight during the assay, probably denoting the adversal consequences of metastases in lungs and liver. In contrast, stauprimide treated animals remain in a constant body weight during the assay, indicating the lack of toxicity of the compound and suggesting better health conditions of these mice compared to DMSO-group.

Additionally, we observed that p38-MAPK pathway was overactivated in stauprimide-treated MDA-MB-231 cells. The activation of this pathway occurs in response to environmental and genotoxic stresses, leading to different cellular fates, such as apoptosis, terminal differentiation, or senescence. In fact, p38 has been described to modulate tissue homeostasis through the promotion of cell differentiation while negative controlling proliferation in many cell types [33,34]. Although it was initially considered as a tumor-supressor kinase due to the negative modulation exerted on Ras signaling [35], in the last years, a dual role for p38-MAPK in tumorigenesis has been proposed, since it has been described as a tumor-promoter protein in certain cancer types and tumoral contexts [33,36]. Interestingly, and in accordance with the activation of the pathway observed in stauprimide-treated MDA-MB-231 cells, p38-MAPK regulates cell cycle activating checkpoint responses at both G_1/S and G_2/M phases [37–39], and the sustained activation of p38-MAPK has been described to suppress mammary tumorigenesis through activation of p16 pathway [40]. In addition, the overexpression of PPM1D (Protein Phosphatase, Mg2 +/Mn2 + Dependent, 1D), a negative regulator of p38-MAPK, has been documented in breast cancer [41], suggesting that the observed activation of this pathway in MDA-MB-231 in presence of stauprimide could contribute to the anti-tumoral effect of this compound in TNBC. Additionally, the activation of p38-MAPK pathway has been reported to be a key axis in the promotion of cell senescence [42,43]. The showed overactivation of this pathway in stauprimide-treated MDA-MB-231 could drive in these cells the senescence-like behaviour observed in presence of the compound, an underlayer mechanism that has been observed for antitumoral agents in other cancer contexts [20,44]. Interestingly, the histology of breast tumors derived from the animal models used in this work showed an increase in the necrotic core of the tumoral mass when animals were treated with stauprimide, which could fit with the induction of senescence-associated cell death in cancer cells.

In this work, we showed that stauprimide reduced the expression of *MYC,* together with a decrease in CMYC protein, in MDA-MB-231 cells, as previously described [8]. CMYC is a very pleiotropic transcription factor involved in a high variety of physiological processes in cells, such as cell-fate patterning, proliferation, migration and survival, among others, being a known protoncogene [7]. Its role in cell cycle progression has been largely studied, being related to several cell cycle checkpoints and antagonizing the activity of cell cycle inhibitors such as p21 and p27 [45]. Indeed, the showed G_2/M arrest of MDA-MB-231 cells in presence of stauprimide could be a consequence of the reduction in CMYC, since the depletion of this protein in several tumor cell lines has been described to result in a blockage of cell cycle in this phase [46]. Nevertheless, we did not observe an induction in $p27^{Kip1}$ in parallel with CMYC downregulation, despite the documented suppressing role of CMYC in *p27* expression in breast cancer [47,48]. Interestingly, stauprimide has been described as an enhancer of differentiation in ESCs *in vitro*, being a potent inhibitor of *MYC* expression through a mechanism involving the blockage of nuclear translocation of the protein NME2 [3]. Although the existence of a NME2-driven inhibitory effect in *MYC* expression in MDA-MB-231 cells treated with stauprimide can not been discarded, our data showed the downregulation of both PI3K/Akt and ERK1/2 MAPK pathways in response to the compound, suggesting that these effects could contribute to the observed CMYC reduction in these cells in response to stauprimide. In fact, *MYC* expression, protein stabilization and activity are promoted by the Ras/Raf/ERK pathway [49] and by GSK3, a known downstream target of the PI3K/Akt pathway [24,50], suggesting that the inhibition of these pathways could be sufficient to downregulate CMYC in breast cancer cells in presence of stauprimide.

Although the exact mechanism of action of stauprimide in TNBC cells is not fully elucidated in this work, the differential modulation in signalling pathways observed in MDA-MB-231 and MCF7 in response to stauprimide could underly the difference in cell survival observed in TNBC cell lines compared to MCF7 breast cancer cells. Our data suggest that activation of PI3K/Akt survival pathway in stauprimide-treated MCF7 cells could be buffering the antiproliferative effect of the compound, in contrast with the more pronounced effect achieved in MDA-MB-231, where PI3K/Akt pathway is downregulated. Regarding *MYC* expression, the level of CMYC has been found to be elevated in TNBC tumors [51,52]. This is also the case for TNBC cell lines, especially MDA-MB-231 compared to other TNBC cell lines [52]. However, we show that the expression of *MYC* is similar in MDA-MB-231 and MCF7 cells, and stauprimide is able to reduce this expression in both cell lines, suggesting that the observed differential effect of stauprimide on MDA-MB-231 cell growth compared to that on MCF7 is not due to differences in CMYC regulation.

5. Conclusions

In conclusion, data presented in this work point to the promising role of stauprimide as a therapeutic agent in TNBC. Although the exact mechanism of action of this compound underlying its antitumoral and anti-metastatic activities needs to be fully elucidated, our *in vitro* results point out an important reduction in cell proliferation together with cell cycle arrest in G_2/M, probably driven by the inhibition in ERK1/2 MAPK and PI3K/Akt pathways, together with the downregulation in *MYC* expression. Additionally, the overactivation of the p38-MAPK pathway could suggest the activation of senescence-induced cell death in TNBC cells and tumors in response to stauprimide, which remains to be explored. The effect of the compound inhibiting migration *in vitro* could be related to the observed anti-metastatic effect *in vivo*, and the exact

mechanism of action of stauprimide in this activity remains to be explored. Although more extensive studies should be performed in order to unveil the antitumoral effect of stauprimide in TNBC, including its anti-metastatic effect, its role in senescence induction, or the efficiency of the combined therapies with chemotherapeutic drugs, our work suggests a potential of this compound in cancer treatment, opening an unexplored therapeutic pathway for TNBC.

Funding

This work was supported by grants PID2019-105010RB-I00 (MICINN and FEDER, Spain), UMA18-FEDERJA-220 and PY20_00257 (Andalusian Government and FEDER, Spain), and funds from "Ayudas Plan Propio IBIMA, 2020″ (IBIMA-Plataforma BIONAND, Spain) and from group BIO 267 (Andalusian Government, Spain), CTQ2017-86655-R (MINECO and FEDER, Spain), PID2020-118448RB-C21 (MICINN and FEDER, Spain) and P20_00727 (Andalusian Government and FEDER, Spain). The "CIBER de Enfermedades Raras", "CIBER de Enfermedades Cardiovasculares" and the "Biomedical Research Networking Center in Bioingineering, Biomaterials and Nanomedicine" are initiatives from the ISCIII (Spain). P.C. was supported by a postdoctoral fellow of Andalusian Government, Spain; M.B. is supported by "Juan de la Cierva – Incorporation Program" (IJC2018-037657-I), Spanish Ministry of Science and Innovation, Spain. The funders had no role in the study design, data collection and analysis, decision to publish or preparation of the manuscript.

CRediT authorship contribution statement

Carrillo, P.: Investigation, Formal analysis, Writing – Original draft, Writting – Review and editing, Visualization **Bernal, M.:** Methodology, Investigation, Formal analysis, Writting – Review and editing, Visualization **Téllez-Quijorna, C.:** Investigation, Formal analysis, Writing – Original draft **Marrero, A.D.:** Investigation **Vidal, I.:** Investigation **Castilla, L.:** Investigation **Caro, C.:** Methodology, Investigation, Writting – Review and editing, Visualization **Domínguez, A.:** Methodology, Investigation **García-Martín, M.L.:** Methodology, Writting – Review and editing, Supervision, Funding acquisition **Quesada, A.R.:** Writting – Review and editing, Funding acquisition **Medina, M.A.:** Conceptualization, Writting – Review and editing, Supervision, Funding acquisition **Martínez-Poveda, B.:** Conceptualization, Methodology, Formal analysis, Writing – Original draft, Writting – Review and editing, Visualization, Supervision, Funding acquisition.

Conflict of Interest statement

The authors declare that they have no known competing financial interests or personal relationships that could have appeared to influence the work reported in this paper.

Acknowledgements

MRI experiments were performed in the ICTS "NANBIOSIS", more specifically in the U28 Unit at the Andalusian Centre for Nanomedicine & Biotechnology (BIONAND). Cell cultures were performed in the Cell Culture Service at the Central Support Services of Research (SCAI) of the University of Málaga. Partial funding for open access charge: Universidad de Málaga / CBUA.

Appendix A. Supporting information

Supplementary data associated with this article can be found in the online version at doi:10.1016/j.biopha.2022.114070.

References

[1] H. Sung, J. Ferlay, R.L. Siegel, M. Laversanne, I. Soerjomataram, A. Jemal, F. Bray, Global Cancer Statistics 2020: GLOBOCAN estimates of incidence and mortality worldwide for 36 cancers in 185 countries, CA Cancer J. Clin. 71 (2021) 209–249, https://doi.org/10.3322/caac.21660.

[2] M. Ensenyat-Mendez, P. Llinàs-Arias, J.I.J. Orozco, S. Íñiguez-Muñoz, M. P. Salomon, B. Sesé, M.L. DiNome, D.M. Marzese, Current triple-negative breast cancer subtypes: dissecting the most aggressive form of breast cancer, Front Oncol. 11 (2021), https://doi.org/10.3389/fonc.2021.681476.

[3] S. Zhu, H. Wurdak, J. Wang, C.A. Lyssiotis, E.C. Peters, C.Y. Cho, X. Wu, P. G. Schultz, A small molecule primes embryonic stem cells for differentiation, Cell Stem Cell 4 (2009) 416–426, https://doi.org/10.1016/j.stem.2009.04.001.

[4] J.A. Byrne, S.M. Mitalipov, L. Clepper, D.P. Wolf, Transcriptional profiling of rhesus monkey embryonic stem cells, Biol. Reprod. 75 (2006) 908–915, https://doi.org/10.1095/biolreprod.106.053868.

[5] G.S. Puts, M.K. Leonard, N. v Pamidimukkala, D.E. Snyder, D.M. Kaetzel, Nuclear functions of NME proteins, Lab. Investig. 98 (2018) 211–218, https://doi.org/10.1038/labinvest.2017.109.

[6] P. Cartwright, C. McLean, A. Sheppard, D. Rivett, K. Jones, S. Dalton, LIF/STAT3 controls ES cell self-renewal and pluripotency by a Myc-dependent mechanism, Development 132 (2005) 885–896, https://doi.org/10.1242/dev.01670.

[7] C. v Dang, MYC on the path to cancer, Cell 149 (2012) 22–35, https://doi.org/10.1016/j.cell.2012.03.003.

[8] C. Bouvard, S.M. Lim, J. Ludka, N. Yazdani, A.K. Woods, A.K. Chatterjee, P. G. Schultz, S. Zhu, Small molecule selectively suppresses MYC transcription in cancer cells, Proc. Natl. Acad. Sci. U. S. A. 114 (2017) 3497–3502, https://doi.org/10.1073/pnas.1702663114.

[9] X. Dai, H. Cheng, Z. Bai, J. Li, Breast cancer cell line classification and its relevance with breast tumor subtyping, J. Cancer 8 (2017) 3131–3141, https://doi.org/10.7150/jca.18457.

[10] B. Schrörs, S. Boegel, C. Albrecht, T. Bukur, V. Bukur, C. Holtsträter, C. Ritzel, K. Manninen, A.D. Tadmor, M. Vormehr, U. Sahin, M. Löwer, Multi-omics characterization of the 4T1 murine mammary gland tumor model, Front Oncol. 10 (2020), https://doi.org/10.3389/fonc.2020.01195.

[11] S. Rodríguez-Nieto, M. González-Iriarte, R. Carmona, R. Muñoz-Chápuli, M. A. Medina, A.R. Quesada, Antiangiogenic activity of aeroplysinin-1, a brominated compound isolated from a marine sponge, FASEB J. 16 (2002) 1–27, https://doi.org/10.1096/fj.01-0427fje.

[12] B. Martínez-Poveda, J.A. García-Vilas, C. Cárdenas, E. Melgarejo, A.R. Quesada, M. A. Medina, The brominated compound aeroplysinin-1 inhibits proliferation and the expression of key pro- inflammatory molecules in human endothelial and monocyte cells, PLoS One 8 (2013), e55203, https://doi.org/10.1371/journal.pone.0055203.

[13] J. Schindelin, I. Arganda-Carreras, E. Frise, V. Kaynig, M. Longair, T. Pietzsch, S. Preibisch, C. Rueden, S. Saalfeld, B. Schmid, J.-Y. Tinevez, D.J. White, V. Hartenstein, K. Eliceiri, P. Tomancak, A. Cardona, Fiji: an open-source platform for biological-image analysis, Nat. Methods 9 (2012) 676–682, https://doi.org/10.1038/nmeth.2019.

[14] B.R. Barricelli, E. Casiraghi, J. Gliozzo, V. Huber, B.E. Leone, A. Rizzi, B. Vergani, ki67 nuclei detection and ki67-index estimation: a novel automatic approach based on human vision modeling, BMC Bioinforma. 20 (2019) 733, https://doi.org/10.1186/s12859-019-3285-4.

[15] C. v Dang, K.A. O'Donnell, K.I. Zeller, T. Nguyen, R.C. Osthus, F. Li, The c-Myc target gene network, Semin Cancer Biol. 16 (2006) 253–264, https://doi.org/10.1016/j.semcancer.2006.07.014.

[16] W. Yang, J. Shen, M. Wu, M. Arsura, M. FitzGerald, Z. Suldan, D.W. Kim, C. S. Hofmann, S. Pianetti, R. Romieu-Mourez, L.P. Freedman, G.E. Sonenshein, Repression of transcription of the p27(Kip1) cyclin-dependent kinase inhibitor gene by c-Myc, Oncogene 20 (2001) 1688–1702, https://doi.org/10.1038/sj.onc.1204245.

[17] K. Tao, M. Fang, J. Alroy, G.G. Gary, Imagable 4T1 model for the study of late stage breast cancer, BMC Cancer 8 (2008), https://doi.org/10.1186/1471-2407-8-228.

[18] D.L. Holliday, V. Speirs, Choosing the right cell line for breast cancer research, Breast Cancer Res. 13 (2011) 215, https://doi.org/10.1186/bcr2889.

[19] J.D. Orth, A. Loewer, G. Lahav, T.J. Mitchison, Prolonged mitotic arrest triggers partial activation of apoptosis, resulting in DNA damage and p53 induction, Mol. Biol. Cell 23 (2012) 567–576, https://doi.org/10.1091/mbc.E11-09-0781.

[20] R. Haq, J.D. Brenton, M. Takahashi, D. Finan, A. Finkielsztein, S. Damaraju, R. Rottapel, B. Zanke, Constitutive p38HOG mitogen-activated protein kinase activation induces permanent cell cycle arrest and senescence, Cancer Res. 62 (2002) 5076–5082.

[21] A.A. Marusiak, Z.C. Edwards, W. Hugo, E.W. Trotter, M.R. Girotti, N.L. Stephenson, X. Kong, M.G. Gartside, S. Fawdar, A. Hudson, W. Breitwieser, N.K. Hayward, R. Marais, R.S. Lo, J. Brognard, Mixed lineage kinases activate MEK independently of RAF to mediate resistance to RAF inhibitors, Nat. Commun. 5 (2014) 3901, https://doi.org/10.1038/ncomms4901.

[22] D.S. Dorow, L. Devereux, E. Dietzsch, T. de Kretser, Identification of a new family of human epithelial protein kinases containing two leucine/isoleucine-zipper domains, Eur. J. Biochem 213 (1993) 701–710, https://doi.org/10.1111/j.1432-1033.1993.tb17810.x.

[23] C.J. Caunt, M.J. Sale, P.D. Smith, S.J. Cook, MEK1 and MEK2 inhibitors and cancer therapy: the long and winding road, Nat. Rev. Cancer 15 (2015) 577–592, https://doi.org/10.1038/nrc4000.

[24] J. Luo, B.D. Manning, L.C. Cantley, Targeting the PI3K-Akt pathway in human cancer, Cancer Cell 4 (2003) 257–262, https://doi.org/10.1016/S1535-6108(03)00248-4.
[25] J. Yang, J. Nie, X. Ma, Y. Wei, Y. Peng, X. Wei, Targeting PI3K in cancer: mechanisms and advances in clinical trials, Mol. Cancer 18 (2019) 26, https://doi.org/10.1186/s12943-019-0954-x.
[26] J. Pascual, N.C. Turner, Targeting the PI3-kinase pathway in triple-negative breast cancer, Ann. Oncol. 30 (2019) 1051–1060, https://doi.org/10.1093/annonc/mdz133.
[27] S. Zhu, H. Wurdak, J. Wang, C.A. Lyssiotis, E.C. Peters, C.Y. Cho, X. Wu, P. G. Schultz, A small molecule primes embryonic stem cells for differentiation, Cell Stem Cell 4 (2009) 416–426, https://doi.org/10.1016/j.stem.2009.04.001.
[28] Y. Ma, J. Shepherd, D. Zhao, L.R. Bollu, W.M. Tahaney, J. Hill, Y. Zhang, A. Mazumdar, P.H. Brown, SOX9 is essential for triple-negative breast cancer cell survival and metastasis, Mol. Cancer Res. 18 (2020) 1825–1838, https://doi.org/10.1158/1541-7786.MCR-19-0311.
[29] M. Nedeljković, A. Damjanović, Mechanisms of chemotherapy resistance in triple-negative breast cancer-how we can rise to the challenge, Cells 8 (2019) 957, https://doi.org/10.3390/cells8090957.
[30] K.A. Mouchemore, R.L. Anderson, J.A. Hamilton, Neutrophils, G-CSF and their contribution to breast cancer metastasis, FEBS J. 285 (2018) 665–679, https://doi.org/10.1111/febs.14206.
[31] F.R. Greten, S.I. Grivennikov, Inflammation and cancer: triggers, mechanisms, and consequences, Immunity 51 (2019) 27–41, https://doi.org/10.1016/j.immuni.2019.06.025.
[32] B.M. Allen, K.J. Hiam, C.E. Burnett, A. Venida, R. DeBarge, I. Tenvooren, D. M. Marquez, N.W. Cho, Y. Carmi, M.H. Spitzer, Systemic dysfunction and plasticity of the immune macroenvironment in cancer models, Nat. Med. 26 (2020) 1125–1134, https://doi.org/10.1038/s41591-020-0892-6.
[33] A. Martínez-Limón, M. Joaquin, M. Caballero, F. Posas, E. de Nadal, The p38 pathway: from biology to cancer therapy, Int. J. Mol. Sci. 21 (2020) 1913, https://doi.org/10.3390/ijms21061913.
[34] B. Canovas, A.R. Nebreda, Diversity and versatility of p38 kinase signalling in health and disease, Nat. Rev. Mol. Cell Biol. 22 (2021) 346–366, https://doi.org/10.1038/s41580-020-00322-w.
[35] G. Chen, M. Hitomi, J. Han, D.W. Stacey, The p38 pathway provides negative feedback for ras proliferative signaling, J. Biol. Chem. 275 (2000) 38973–38980, https://doi.org/10.1074/jbc.M002856200.
[36] J. Gupta, I. del Barco Barrantes, A. Igea, S. Sakellariou, I.S. Pateras, V.G. Gorgoulis, A.R. Nebreda, Dual function of p38α mapk in colon cancer: suppression of colitis-associated tumor initiation but requirement for cancer cell survival, Cancer Cell 25 (2014) 484–500, https://doi.org/10.1016/j.ccr.2014.02.019.
[37] L. Stramucci, A. Pranteda, G. Bossi, Insights of crosstalk between p53 protein and the MKK3/MKK6/p38 MAPK signaling pathway in cancer, Cancers (Basel) 10 (2018) 131, https://doi.org/10.3390/cancers10050131.
[38] V. Lafarga, A. Cuadrado, I. Lopez de Silanes, R. Bengoechea, O. Fernandez-Capetillo, A.R. Nebreda, p38 mitogen-activated protein kinase- and hur-dependent stabilization of p21 Cip1 mRNA mediates the G 1 /S checkpoint, Mol. Cell Biol. 29 (2009) 4341–4351, https://doi.org/10.1128/mcb.00210-09.
[39] M. Raman, S. Earnest, K. Zhang, Y. Zhao, M.H. Cobb, TAO kinases mediate activation of p38 in response to DNA damage, EMBO J. 26 (2007) 2005–2014, https://doi.org/10.1038/sj.emboj.7601668.
[40] D. v Bulavin, C. Phillips, B. Nannenga, O. Timofeev, L.A. Donehower, C. W. Anderson, E. Appella, A.J. Fornace, Inactivation of the Wip1 phosphatase inhibits mammary tumorigenesis through p38 MAPK-mediated activation of the p16Ink4a-p19 Arf pathway, Nat. Genet. 36 (2004) 343–350, https://doi.org/10.1038/ng1317.
[41] J. Li, Y. Yang, Y. Peng, R.J. Austin, W.G. van Eyndhoven, K.C.Q. Nguyen, T. Gabriele, M.E. McCurrach, J.R. Marks, T. Hoey, S.W. Lowe, S. Powers, Oncogenic properties of PPM1D located within a breast cancer amplification epicenter at 17q23, Nat. Genet. 31 (2002) 133–134, https://doi.org/10.1038/ng888.
[42] L. Wang, L. Lankhorst, R. Bernards, Exploiting senescence for the treatment of cancer, Nat. Rev. Cancer 22 (2022) 340–355, https://doi.org/10.1038/s41568-022-00450-9.
[43] H. Iwasa, J. Han, F. Ishikawa, Mitogen-activated protein kinase p38 defines the common senescence-signalling pathway, Genes Cells 8 (2003) 131–144, https://doi.org/10.1046/j.1365-2443.2003.00620.x.
[44] P.L. Puri, Z. Wu, P. Zhang, L.D. Wood, K.S. Bhakta, J. Han, J.R. Feramisco, M. Karin, J.Y. Wang, Induction of terminal differentiation by constitutive activation of p38 MAP kinase in human rhabdomyosarcoma cells, Genes Dev. 14 (2000) 574–584. ⟨http://www.ncbi.nlm.nih.gov/pubmed/10716945⟩.
[45] G. Bretones, M.D. Delgado, J. León, Myc and cell cycle control, Biochim Biophys. Acta Gene Regul. Mech. 2015 (1849) 506–516, https://doi.org/10.1016/j.bbagrm.2014.03.013.
[46] H. Wang, S. Mannava, V. Grachtchouk, D. Zhuang, M.S. Soengas, A. v Gudkov, E. v Prochownik, M.A. Nikiforov, c-Myc depletion inhibits proliferation of human tumor cells at various stages of the cell cycle, Oncogene 27 (2008) 1905–1915, https://doi.org/10.1038/sj.onc.1210823.
[47] W. Yang, J. Shen, M. Wu, M. Arsura, M. FitzGerald, Z. Suldan, D.W. Kim, C. S. Hofmann, S. Pianetti, R. Romieu-Mourez, L.P. Freedman, G.E. Sonenshein, Repression of transcription of the p27(Kip1) cyclin-dependent kinase inhibitor gene by c-Myc, Oncogene 20 (2001) 1688–1702, https://doi.org/10.1038/sj.onc.1204245.
[48] V. Chandramohan, N.D. Mineva, B. Burke, S. Jeay, M. Wu, J. Shen, W. Yang, S. R. Hann, G.E. Sonenshein, c-Myc represses FOXO3a-mediated transcription of the gene encoding the p27Kip1 cyclin dependent kinase inhibitor, J. Cell Biochem. 104 (2008) 2091–2106, https://doi.org/10.1002/jcb.21765.
[49] F. Marampon, C. Ciccarelli, B.M. Zani, Down-regulation of c-Myc following MEK/ERK inhibition halts the expression of malignant phenotype in rhabdomyosarcoma and in non muscle-derived human tumors, Mol. Cancer 5 (2006) 31, https://doi.org/10.1186/1476-4598-5-31.
[50] R. Sears, F. Nuckolls, E. Haura, Y. Taya, K. Tamai, J.R. Nevins, Multiple Ras-dependent phosphorylation pathways regulate Myc protein stability, Genes Dev. 14 (2000) 2501–2514, https://doi.org/10.1101/gad.836800.
[51] M.C. Alles, M. Gardiner-Garden, D.J. Nott, Y. Wang, J.A. Foekens, R.L. Sutherland, E.A. Musgrove, C.J. Ormandy, Meta-analysis and gene set enrichment relative to er status reveal elevated activity of MYC and E2F in the “basal” breast cancer subgroup, PLoS One 4 (2009), e4710, https://doi.org/10.1371/journal.pone.0004710.
[52] D. Horiuchi, L. Kusdra, N.E. Huskey, S. Chandriani, M.E. Lenburg, A.M. Gonzalez-Angulo, K.J. Creasman, A. v Bazarov, J.W. Smyth, S.E. Davis, P. Yaswen, G.B. Mills, L.J. Esserman, A. Goga, MYC pathway activation in triple-negative breast cancer is synthetic lethal with CDK inhibition, J. Exp. Med. 209 (2012) 679–696, https://doi.org/10.1084/jem.20111512.